

# RSC Advances



This is an *Accepted Manuscript*, which has been through the Royal Society of Chemistry peer review process and has been accepted for publication.

*Accepted Manuscripts* are published online shortly after acceptance, before technical editing, formatting and proof reading. Using this free service, authors can make their results available to the community, in citable form, before we publish the edited article. This *Accepted Manuscript* will be replaced by the edited, formatted and paginated article as soon as this is available.

You can find more information about *Accepted Manuscripts* in the [Information for Authors](#).

Please note that technical editing may introduce minor changes to the text and/or graphics, which may alter content. The journal's standard [Terms & Conditions](#) and the [Ethical guidelines](#) still apply. In no event shall the Royal Society of Chemistry be held responsible for any errors or omissions in this *Accepted Manuscript* or any consequences arising from the use of any information it contains.



# Production of clinoptilolite nanorods by glow discharge plasma technique for heterogeneous catalytic ozonation of nalidixic acid

Received 00th January 2015,  
Accepted 00th January 2015

DOI: xxxxxxxx

www.rsc.org/

Alireza Khataee<sup>a\*</sup>, Tannaz Sadeghi Rad<sup>a</sup>, Mehrangiz Fathinia<sup>a</sup>, Sang Woo Joo<sup>b\*\*</sup>

This study investigated nalidixic acid degradation via heterogeneous catalytic ozonation using clinoptilolite nanorods (CNs) as a novel nanocatalyst. Natural clinoptilolite microparticles (NCMs) were treated by glow discharge plasma technique (GDP) to generate nanostructures. SEM, EDX, XRD, FT-IR, XPS, and BET were used to elucidate the morphology, chemical composition, and the microstructural properties of the NCMs and CNs. The SEM images of the untreated and plasma-treated clinoptilolite clarified that the morphology of the NCMs was converted to nanorods using the GDP technique. The catalytic performance of the NCMs and CNs in the heterogeneous catalytic ozonation of nalidixic acid was compared. The results demonstrate that in 60 min of the process, the removal efficiency is enhanced from 60.03% in the presence of NCMs to 91.08% when using the CNs. The effect of the main operational parameters and various reactive oxygen species (ROS) scavengers on the removal efficiency of nalidixic acid were thoroughly investigated. The main degradation by-products produced in the catalytic ozonation of nalidixic acid were identified by GC-MS technique. The ecotoxicity of nalidixic acid and the intermediate compounds formed in the process were evaluated using the aquatic species *Lemna minor* (*L. minor*).

**Keywords:** Natural clinoptilolite; Glow discharge plasma; Nanorod; Ozonation; Nalidixic acid.

## 1. Introduction

Synthetic pharmaceutical compounds (SPCs) constitute a vast group of human and veterinary medicinal compounds.<sup>1, 2</sup> SPCs appear to be the main class of water contaminants due to their wide consumption and unknown biological and phyto-toxicological effects. These toxic pollutants are constantly released into the environment from hospital wastes and industrial and domestic sites. Consequently, they are detected in wastewater, surface water, and even drinking water.<sup>3</sup>

Many SPCs are resistant to natural degradation, biodegradation, and photo-transformation.<sup>4</sup> Therefore, they can stay in water bodies for an extended period of time and can give rise to aquatic toxicity, endocrine disruption, and genotoxicity.<sup>5, 6</sup> Hence, over the past few years, SPCs have been considered a prime environmental problem. Comprehensive studies have been performed to introduce novel and efficient degradation methods for removal of SPCs from water bodies.<sup>5</sup> Nalidixic acid is a non-fluorinated quinolone antibacterial agent for oral administration. It is one of the most regularly

identified SPCs in water sources. It is not entirely degraded during wastewater treatment processes and thus enters surface waters.<sup>7</sup>

In recent decades, advanced oxidation processes (AOPs) have been regarded as effective methods for the removal of SPCs from bodies of water via the production of ROSs such as hydroxyl radicals ( $E^\circ = 2.6$  eV).<sup>8</sup> Recently, ozonation has become well known as a rapid method to remove toxic organic contaminants from wastewaters.<sup>9</sup> However, the utilization of a single ozonation process in water treatment steps might not be beneficial due to limitations of low solubility and stability of ozone in water and high costs of instruments for industrial production of ozone, which is able to partially degrade the organic pollutants.<sup>10-12</sup>

Most of the research has focused on catalytic ozonation as an AOP to resolve the obstacles related to a single ozonation process.<sup>13</sup> Enhanced production of oxidant species (such as hydroxyl radicals) and increased degradation and mineralization of organic pollutants are regarded as prominent advantages of catalytic ozonation in comparison with a traditional non-catalytic process.<sup>14, 15</sup> A catalytic ozonation process can be performed in either homogeneous or heterogeneous modes.<sup>16</sup> In homogeneous catalytic ozonation, the catalytic effects are due to the presence of soluble metal ions.<sup>17</sup> In heterogeneous catalytic ozonation, the oxidation reaction can simultaneously occur on both the surface of the solid catalyst and in the bulk water.<sup>18</sup>

The most promising catalyst, clinoptilolite, has been immensely utilized in various catalytic processes due to its abundance and low cost. In addition, clinoptilolite is not toxic and thus attracts researchers' interest as a green catalyst.<sup>19</sup> Despite these unique properties, low specific surface area limits clinoptilolite usage. In the case of heterogeneous catalytic ozonation, reaction between various

<sup>a</sup> Research Laboratory of Advanced Water and Wastewater Treatment Processes, Department of Applied Chemistry, Faculty of Chemistry, University of Tabriz, 51666-16471 Tabriz, Iran.

<sup>b</sup> School of Mechanical Engineering, Yeungnam University, 712-749 Gyeongsan, South Korea

\*Corresponding author (communicator)

E-mail address: a\_khataee@tabrizu.ac.ir (ar\_khataee@yahoo.com)

Tel.: +98 41 33393165; Fax: +98 41 33340191

\*\*Co-corresponding author

E-mail address: swjoo@yu.ac.kr

Tel: +82 53 810 1456

types of organic compounds such as pharmaceuticals, ozone, and hydroxyl radicals proceed on the surface of a catalyst. High specific surface area of the catalyst is thus predicted to be a basic factor for catalysis application.<sup>20</sup> Low specific surface area decreases the reaction rate of catalytic ozonation. Therefore, to overcome the limitations, some methods have been devised to enhance the catalyst specific surface area, which leads to higher reaction rate of the process.

Nanomaterials contain high specific surface area.<sup>18, 21-23</sup> Therefore, it is anticipated that nanosized clinoptilolite would be appropriate for heterogeneous catalytic processes such as ozonation due to high specific surface area. Different synthetic techniques have been used to synthesize zeolites with nanostructure. However, issues such as toxicity of the precursors, high costs, and complexity of the synthesis procedure have limited the wide utilization of these methods.<sup>24, 25</sup> Recently, nonthermal plasma techniques have been introduced as simple and green methods for modification of catalyst surfaces and production of various nanomaterials. Examples are radio frequency (RF) discharge, glow discharge, and silent discharge.<sup>21, 26, 27</sup>

In the present study, CNs were prepared using of the GDP technique. The physical and chemical characteristics of NCMs and CNs were investigated by scanning electron microscopy (SEM), energy-dispersive X-ray spectroscopy (EDX), X-ray diffraction (XRD), Fourier transform infrared spectroscopy (FT-IR), X-ray photoelectron spectroscopy (XPS), and Brunauer-Emmett-Teller (BET) analysis. Then, the obtained CNs were used as a novel nanocatalyst in the heterogeneous catalytic ozonation process for removal of nalidixic acid. A thorough investigation was performed on the effect of operational variables involving the effect of ozone inlet flow rate, catalyst concentration, pH, and nalidixic acid concentration.

The oxidation mechanism of the heterogenous catalytic ozonation process was examined by monitoring the concentration of dissolved ozone in various oxidation processes and by using selective radical scavengers. The degradation by-products of nalidixic acid produced during catalytic ozonation were identified. The chronic ecotoxicity of nalidixic acid and its degradation by-products was evaluated on an aquatic species *L. minor*.

## 2. Experimental

### 2.1. Reagents and materials

All the chemicals supplied by Merck Co. (Germany) were analytical grade and used without purification. Natural clinoptilolite tuffs were purchased from the Mianeh region in the north-west of Iran (Kan Azar Co, Tabriz, Iran). Nalidixic acid was obtained from Rouz Darou Co. (Tehran, Iran).

### 2.2. Plasma-treatment procedure

Figure 1 shows the experimental apparatus used for the plasma-treatment procedure. The main body of the GDP reactor was fabricated from a Pyrex tube with dimensions of 40 cm × 5 cm. An AC power supply (3000 V, Tabriz, Iran) was applied to the two electrodes to generate GDP. About 2 g of dry clinoptilolite powder was placed on a Pyrex plate and fixed in the positive column zone of the GDP reactor. After vacating the reactor, N<sub>2</sub> gas was introduced into the reactor tube at a pressure of 53.3 Pa as the plasma-forming gas. Due to the high voltage of plasma treatment, which is not cost effective for long periods of catalyst treatment, the duration of plasma processing was selected as 60 min. After the plasma-treatment procedure, the CNs were collected for use in the catalytic ozonation of nalidixic acid.

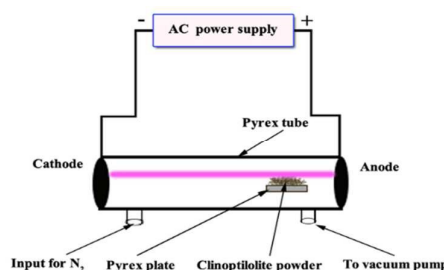


Figure 1. Schematic image of the glow discharge plasma technique reactor used in this study.

### 2.3. Heterogeneous catalytic ozonation procedure

The catalytic ozonation reactions were performed in a semi-batch mode using a cylindrical Pyrex reactor containing a 250-mL aqueous solution of nalidixic acid at atmospheric pressure and ambient temperature. As it can be observed from the schematic diagram of the system presented in Figure 2, the reactor contained an inlet for ozone gas, an outlet for non-absorbed ozone, a sampling port, and a porous ceramic diffuser. The solution inside the reactor was constantly mixed using a magnetic stirrer. Oxygen gas (1-5 L/min) supplied by oxygen generator (Airsep, USA) as a feed gas for the laboratory ozone generator. Ozone gas continuously entered the solution through a diffuser at the bottom of the reactor.

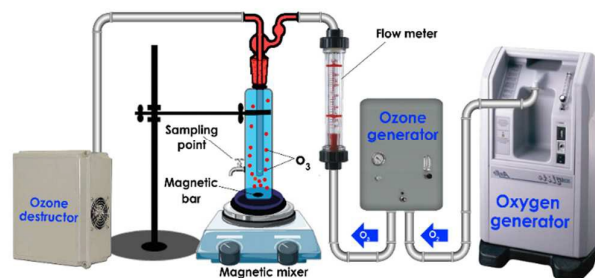


Figure 2. Schematic image of the used ozonation set-up.

The gas flow meter was applied to adjust the ozone flow rate from 1 to 7 L/h. In a typical run, 2 g/L of CNs were put into a 250 mL of an aqueous solution of nalidixic acid (20 mg/L). The solution pH was adjusted with a Metrohm 654 pH meter (Switzerland). At different time intervals, 3 mL of the sample were removed, and the removal efficiency of nalidixic acid was calculated by measuring the absorbance at the maximum wavelength ( $\lambda_{\max} = 330$  nm) using a UV-Vis spectrophotometer (Lightwave S2000, England). The dissolved ozone concentration was determined by the indigo colorimetric method using decoloration of a 5,5,7-indigotrisulphonate solution according to a method by Bader and Hoigné.<sup>28</sup> Different molar ratios with respect to nalidixic acid of ROS scavengers or inorganic ions (1:1, 10:1 and 50:1) were separately added to the nalidixic acid aqueous solution. By adding different ROS scavengers to the system, the role of surface active sites of the catalyst and the radicals involved in the heterogeneous catalytic ozonation were investigated.

### 2.4. Catalysts characterization

To investigate the crystallographic properties of the NCMs and CNs, XRD analysis was applied (PANalytical X'Pert PRO, Germany). XRD analysis was used on the samples with CuK $\alpha$  radiation (45 kV, 40 mA, 0.15406 nm). A quantitative compositional analysis was conducted by XPS measurements using a spectrometer (K-Alpha, Thermo Scientific, U.K.). SEM (Mira3 FEG-SEM, Tescan, Czech) coupled with EDX microanalysis (acceleration

voltage of 10 kV) was applied to determine the morphology and the chemical composition of the samples, respectively. About the preparation of the samples for SEM analysis it should be mentioned that the small amount of samples were mounted on a stub of metal with adhesive, coated with a thin layer of gold metal before SEM examination and then analyzed by SEM apparatus. Manual Microstructure Distance Measurement software (Nahamin Pardazan Asia Co., Iran) was used to determine the size distribution of the sample. The microstructural properties of the samples were investigated by nitrogen sorption analysis with a ChemBET 3000 (Quantachrome, USA) at 77.35 K using calcined samples.

The FT-IR spectra of the samples were recorded using an FT-IR spectrometer (Tensor 27, Bruker, Germany) and the KBr pellet technique. GC-Mass analysis was carried out to identify the intermediates produced during nalidixic acid degradation. 250 mL of nalidixic acid solution (40 mg/L) was treated for 4 min under the optimized conditions. Afterward, to extract the organic compounds from the treated solution, 25 mL of diethyl ether were added three times. After volatilization, the remaining solid was dissolved in 100  $\mu$ L of N, O-bis-(trimethylsilyl)-acetamide with stirring for 10 min and heating at 60  $^{\circ}$ C. The obtained silylated products were analyzed by GC-MS (Agilent 6890 gas chromatography, 5973 mass spectrometer; Palo Alto, Canada). The temperatures of the inlet, transfer line, and detector were 250, 250, and 300  $^{\circ}$ C, respectively.<sup>29</sup> The electron energy was 70 eV.

## 2.5. Ecotoxicological assessment

### 2.5.1. Plant species

Fronds of duckweed (*L. minor*) were obtained from the Anzali Wetland in Northern Iran. Disinfection activities were performed using 0.5% v/v sodium-hypochlorite for 2 min. Afterward, they were washed using distilled water, and modified Steinberg culture medium was applied for cultivation.<sup>30</sup>

### 2.5.2. Phytotoxicity experiments

Catalytic ozonation on 20 mg/L of nalidixic was done in the presence of the CNs under the optimum conditions been obtained from the experiments. At time intervals of 30, 60, 90, and 120 min, 250 mL of treated solution were removed, and 10 mL of nutrient medium were added. The control sample included distilled water and 10 mL of nutrient medium. Twenty major fronds of *L. minor* were added to the solutions, and visual changes in the frond color and colony integrity were monitored by the stereomicroscope (Olympus, Japan).

## 3. Results and discussion

### 3.1. Characterization of plasma-treated clinoptilolite

In the present study, NCMs and CNs were used as heterogeneous catalysts in ozonation process. NCMs were used without any treatment and CNs obtained from modification of NCMs by utilization of GDP technique. SEM images of NCMs and CNs are presented in Figures 3a to 3c. A non-uniform and rough surface was observed on the natural clinoptilolite sample (Figure 3a). Figure 3b and Figure 3c show that uniform and rod-shaped clinoptilolite nanocrystals were generated by the GDP method. The diameter distribution of the CNs is displayed in Figure 3d. The average diameter of the particles was in the range of 20–40 nm.

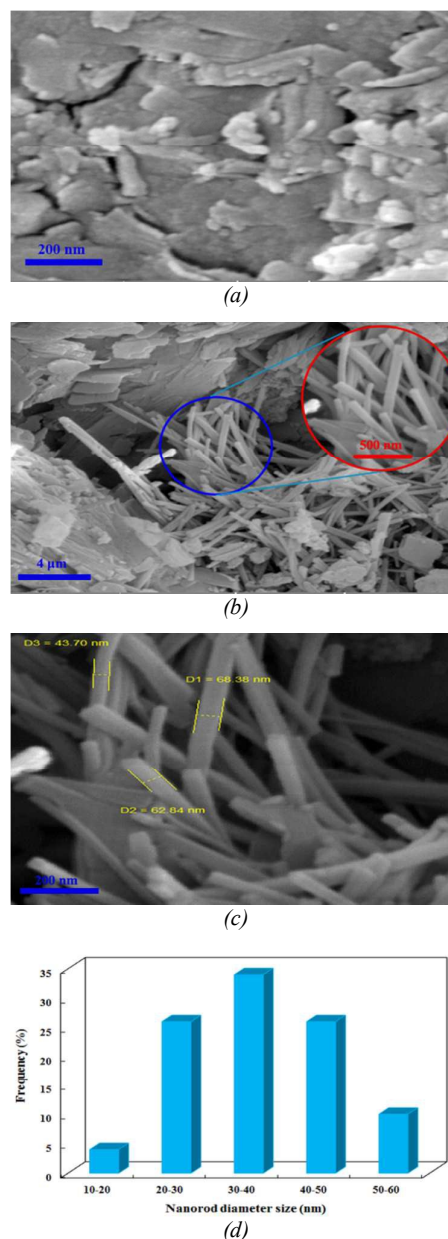


**Figure 3.** SEM images of (a) NCMs, (b and c) CNs with different magnifications, and (d) CN diameter distribution plot.

Figures 4a and 4b indicate the EDX spectra of NCMs and CNs, respectively. EDX analysis was used for determining the chemical elemental composition of the samples. Figure 4a shows the main elements, such as O, Na, Al, Si, and other ions in the NCM structure. The EDX spectrum of the CNs (Figure 4b) shows the main elements of clinoptilolite nanorods. The clinoptilolite nanorods include the same main elements, such as O, Na, Al, and Si.

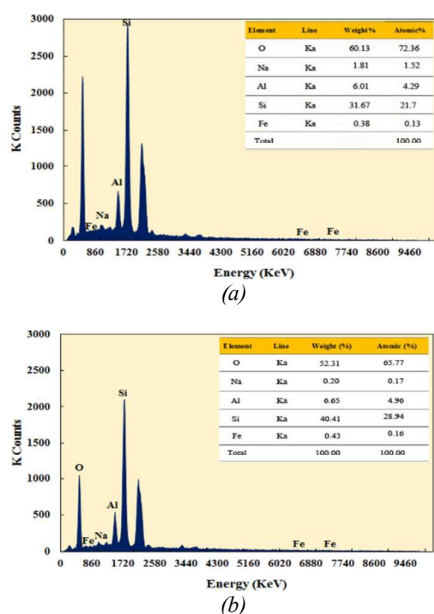


Figure 4. EDX analysis of (a) NCMs and (b) CNs.

From the EDX results, it can be concluded that the chemical composition of NCMs remained unchanged during plasma treatment, and the plasma process did not destroy any of the chemical structure of the samples. It can be proposed that the morphology conversion of the NCMs is due to the effects of oxidation and etching produced during the plasma-treatment procedure.

The X-ray dot mapping of NCMs and CNs are displayed in Figures 5a and 5b. The results display homogenous dispersion of the elements before and after plasma-treatment. In other words, the plasma-treatment procedure did not cause any change in the chemical composition and dispersion of the elements. Therefore, the procedure can be introduced as a promising technique to produce CNs.

Figures 6a and 6b depict the XRD patterns of the NCMs and CNs, respectively. Figure 6a reveals that the four characteristic peaks at  $2\theta$  of  $10.9^\circ$ ,  $17.53^\circ$ ,  $22.7^\circ$ , and  $27.63^\circ$  are in accordance with the data for clinoptilolite (JCPDS card 83-1260).<sup>10, 31</sup> The sharpness of the peaks in Figure 6b after plasma treatment shows structural stability and proper crystallinity of the clinoptilolite after plasma treatment. Therefore, it can be deduced that the GDP procedure did not destroy the clinoptilolite crystal structure.

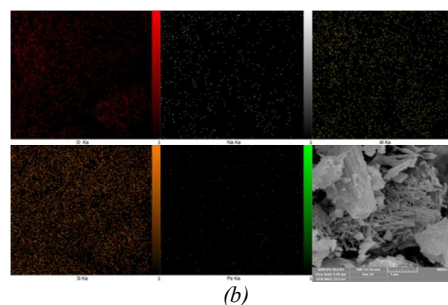
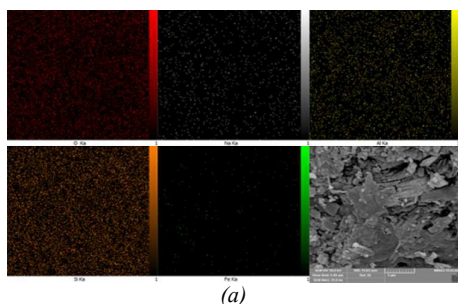


Figure 5. X-Ray dot mapping analysis of major elements for (a) NCMs and (b) CNs.

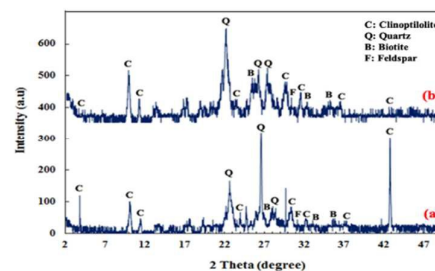
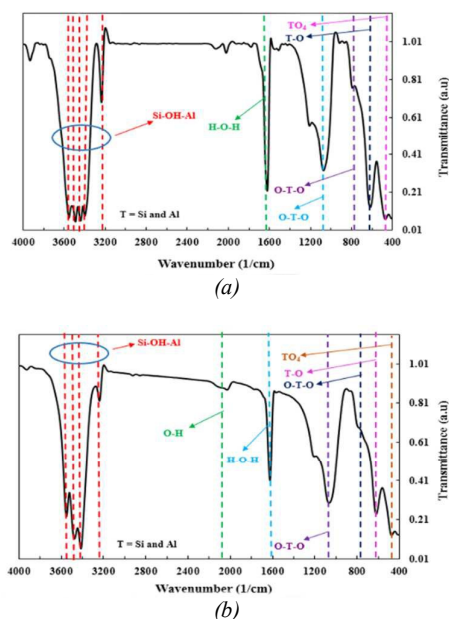


Figure 6. XRD of (a) NCMs and (b) CNs.

FT-IR analysis was used to determine the surface functional groups of the samples. Figures 7a and 7b show the FT-IR spectrum of NCM and CN samples. In Figure 7a, the peak at  $445 \text{ 1/cm}$  is ascribed to the bending of the  $\text{TO}_4$  group inside bonds ( $\text{T}=\text{Si}$  and  $\text{Al}$ ) and symmetric stretching of the free tetrahedral group  $\text{TO}_4$ . The peak at  $611 \text{ 1/cm}$  is ascribed to asymmetric stretching vibrations of  $\text{T}-\text{O}$ . The peaks at  $796$  and  $1046 \text{ 1/cm}$  can be assigned to the asymmetric  $\text{O}-\text{T}-\text{O}$  stretching vibration.<sup>10, 31, 32</sup> Comparison of the FT-IR spectrum of the CNs (Figure 7b) with that of NCMs demonstrates that the main FT-IR vibrations remained unchanged. No obvious replacement or alteration in the intensity of vibrations was detected. Therefore, it can be concluded that the NCM surface functional groups remained unchanged during treatment with the GDP technique.<sup>31</sup>



**Figure 7.** FT-IR spectra of (a) NCMs and (b) CNs.

XPS analysis is highly sensitive for analyzing the catalyst surface chemical species. XPS was utilized to study the chemical states of the cations in NCMs and CNs. This analysis was also applied to determine the energy binding shifting of the framework elements.<sup>33</sup> Figure 8 illustrates the XPS spectra of NCMs and CNs. The results confirm that Al, Si, and O are present in the catalyst structure without any impurities. The peaks at 533.38 eV are related to the O 1s binding energy. The binding energy at 105.00 and 76.96 eV is attributed to Si 2p and Al 2p, respectively. The binding energy of the peaks does not show any significant shift, implying that the elemental distribution of the catalyst remained unchanged. The nitrogen adsorption isotherms were measured using the Brunauer-Emmett-Teller (BET) surface area method to investigate the microstructural properties of the samples.<sup>34</sup> The results showed that the specific surface area of the NCMs increased significantly from 13.35 to 316 m<sup>2</sup>/g after treating with plasma.

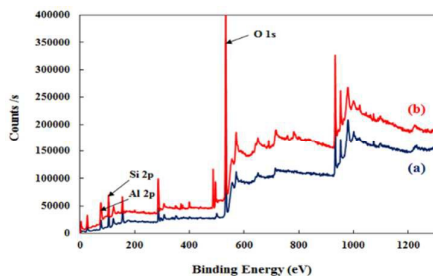


**Figure 8.** XPS spectra of (a) NCMs and (b) CNs.

Based on the results from SEM, EDX, XRD, FT-IR, XPS, and BET analysis and on related literature, the mechanism of the plasma can be proposed. The plasma consists of a mixture of electrons, ions, photons, neutral and excited species.<sup>21</sup> When NCMs are exposed to such an environment, these species could be trapped by the catalyst particles. This phenomenon led to the formation of a plasma sheath around each particle. Consequently, due to the continuous flow of electrons inside the plasma zone, multiple powerful repulsive forces are generated among the plasma sheath, the catalyst particles, and inside the catalyst particles. It is believed that bond deformation between the main elements of the NCMs such as Al, Si, and O can occur due to the mentioned repulsive forces, which leads to morphological changes without altering the main chemical properties of the catalyst. Also, it is hypothesized that the produced repulsive forces are responsible for modification of the microstructural surface properties of the NCMs, which increase the specific surface area.

### 3.2. Comparison of different oxidation processes

It is worth to state that nalidixic acid is a non-fluorinated quinolone anti-bacterial agent with the solubility of 100 mg/mL in water, molecular weight of 232.24 and  $\lambda_{\max}$  of 325 nm. Its molecular structure is given in Figure 9. Figure 10 demonstrates the removal efficiency of nalidixic acid in catalytic ozonation and adsorption processes. It can be observed that the removal of nalidixic acid in the control adsorption tests was about 20% for 60 min. This proves that the adsorption processes in the presence of NCMs and CNs were not able to degrade the nalidixic acid efficiently. Also, the catalytic activity of the plasma-treated catalyst was the highest when comparing nalidixic acid removal by ozonation and the heterogeneous catalytic ozonation process in the presence of NCMs and CNs (see Figure 10). The remarkable difference in the removal efficiency of nalidixic acid using the ozonation process in the presence

of the CN and NCM samples could be due to the microstructural differences of the catalysts.

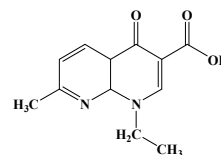


**Figure 9.** Molecular structure of nalidixic acid.

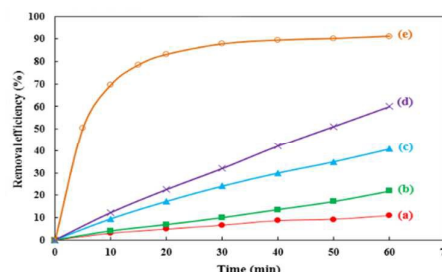


**Figure 10.** Removal efficiency of nalidixic acid in the different processes: (a) adsorption with NCMs, (b) adsorption with CNs, (c) ozonation, (d) catalytic ozonation with NCMs, and (e) catalytic ozonation with CNs (Experimental conditions: [nalidixic acid]<sub>0</sub> = 20 mg/L, ozone inlet flow rate = 7 L/h, [NCMs] = 2 g/L, [CNs] = 2 g/L, and pH = 7).

The results demonstrate that the principal difference between the NCMs and CNs is related to the size and the morphology of the sample particles. Also, as the BET results show, decreasing the size of the particles in the case of CNs leads to an increase in the specific surface area of the catalyst. It can be hypothesized that increasing the specific surface area of the catalyst provides more active sites on the surface of the catalyst. Consequently, this results in an increase in the ozone decomposition on the catalyst surface, and finally, more hydroxyl radicals are formed. So, CNs were chosen as an efficient nanocatalyst, and their performance was studied in the heterogeneous catalytic ozonation process for the degradation of nalidixic acid under different operational parameters such as the ozone inlet flow rate, catalyst concentration, pH, and nalidixic acid concentration. Regarding the degradation of NAD by other oxidation methods it should be stated that Ardo et al. investigated the oxidative capacity of magnetite nanoparticles via heterogeneous Fenton-like reaction for the removal of NAD. Results showed that NAD was firstly adsorbed on the surface of magnetite and then it was degraded. Nearly 60% of NAD was eliminated after 30 min<sup>35</sup>. Also, Petronella et al. reported the UV-induced degradation of the NAD in water matrix by TiO<sub>2</sub> nanorods/Ag nanoparticles<sup>36</sup>. Results showed that 80% of NAD degraded during 60 min of the degradation process<sup>36</sup>. The main novelty of the present study in comparison with others, is the high percentage of the removal efficiency of NAD by catalytic ozonation process, using CNs (91.08% during 60 min). Also, production of CNs by GDP, which is one of the green methods of modification and preparation of nanomaterials is another novelty of the present work.

#### 3.2.1. Effect of ozone inlet flow rate

Figure 11a shows the effect of the ozone inlet flow rate on the removal efficiency of nalidixic acid. Increasing the ozone inlet flow rate in the range of 1 to 7 L/h can improve the removal efficiency. This is due to the increase in concentration of ozone molecules, which can be adsorbed on the active sites of the catalyst. The

adsorbed ozone can be decomposed on the catalyst surface, which results in the production of ROSs such as hydroxyl radicals that are responsible for nalidixic acid degradation in the catalytic ozonation process.<sup>9</sup> Therefore, an ozone inlet flow rate of 7 L/h was selected as the optimum flow rate at which the removal efficiency of the pollutant was the highest.

### 3.2.2. Effect of catalyst concentration

To study the impact of catalyst dosage on the performance of the catalytic ozonation process, experiments were performed with different catalyst concentrations (from 0.4 g/L to 8 g/L). Figure 11b shows that the catalyst concentration has an appreciable positive influence on the removal efficiency of nalidixic acid. The possible reason for the trend is that a high concentration of catalyst provides more surface active sites for more ozone molecules to be decomposed and converted to hydroxyl radicals.<sup>9</sup> However, since the removal efficiency of nalidixic acid in the presence of 2 g/L to 8 g/L did not increase notably, 2 g/L was selected as a suitable optimum concentration from an economic point of view. The potential of clinoptilolite nanorod reusability was also studied by five consecutive experiments carried out in similar conditions. The results show that the clinoptilolite nanorods can be efficiently reused for five cycles as a catalyst without reduction in activity.

### 3.2.3. Effect of the initial solution pH

The influence of the solution pH on the removal efficiency of nalidixic acid is shown in Figure 11c. Hydroxyl radical generation on a catalyst surface is affected by pH.<sup>30, 37</sup> Also, in an ozonation process with enhanced solution pH, more hydroxyl radicals are produced due to improvement in the ozone decomposition.<sup>38</sup>

To further investigate the effect of pH, a nalidixic acid hydrolysis test was performed to determine the effect of pH on the absorbance spectrum of nalidixic acid. The results are presented in Figure 11d, which shows no effects for hydrolysis since the wavelength and absorbance of nalidixic acid were not significantly changed by the solution pH. It can be inferred that the main reason for the increase of nalidixic acid degradation with pH increase is the lower stability of ozone at higher pH.

### 3.2.4. Effect of nalidixic acid concentration

Figure 11e presents the effect of nalidixic acid concentration on the removal efficiency of nalidixic acid in the catalytic ozonation process. The removal efficiency of nalidixic acid was decreased by increasing the nalidixic acid concentration.<sup>39</sup> As the flow rate of ozone is constant in optimum conditions, the amount of  $\cdot\text{OH}$  which produced by ozone decomposition is constant too. When increasing the nalidixic acid concentration, the limited  $\cdot\text{OH}$  will not be able to degrade all of the pollutant molecules. Thus, the removal efficiency is decreased by increasing the nalidixic acid concentration.

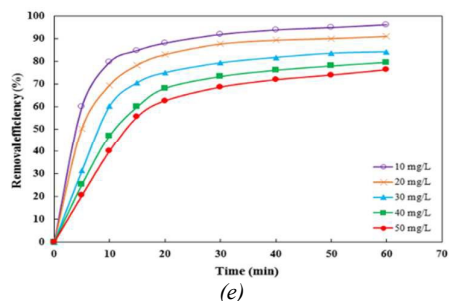
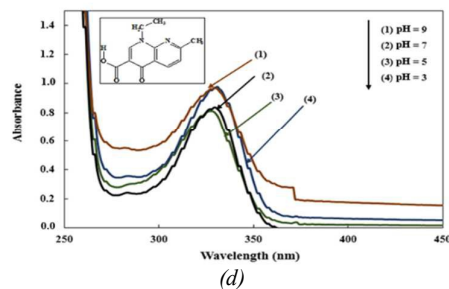
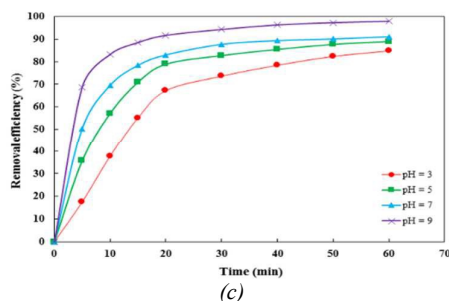
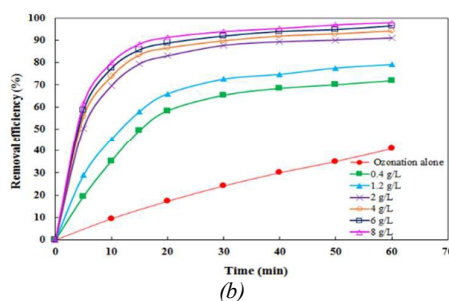
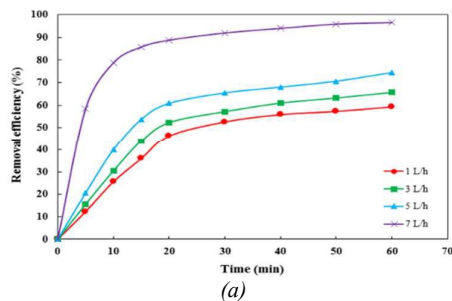


**Figure 11.** (a) Influence of ozone inlet flow rate on the removal efficiency of nalidixic acid (Experimental conditions:  $[\text{nalidixic acid}]_0 = 20 \text{ mg/L}$ ,  $[\text{CNs}] = 6 \text{ g/L}$  and  $\text{pH} = 7$ ); (b) Influence of CNs concentration on the removal efficiency of nalidixic acid (Experimental conditions:  $[\text{nalidixic acid}]_0 = 20 \text{ mg/L}$ , ozone inlet flow rate = 7 L/h and  $\text{pH} = 7$ ); (c) Influence of pH on the removal efficiency of nalidixic acid (Experimental conditions:  $[\text{nalidixic acid}]_0 = 20 \text{ mg/L}$ ,  $[\text{CNs}] = 2 \text{ g/L}$  and ozone inlet flow rate = 7 L/h); (d) Influence of pH on nalidixic acid absorbance spectrum (Experimental conditions:  $[\text{nalidixic acid}]_0 = 20 \text{ mg/L}$ ) and (e) Influence of nalidixic acid concentration on the removal efficiency of nalidixic acid (Experimental conditions: ozone inlet flow rate = 7 L/h,  $[\text{CNs}] = 2 \text{ g/L}$ , and  $\text{pH} = 7$ ).

## 3.3. Mechanism of catalytic ozonation process

### 3.3.1. Concentration of dissolved ozone

The dissolved ozone concentration was evaluated to investigate the mechanism of the catalytic ozonation process. Figure 12 shows that the dissolved ozone concentration is reduced in the catalytic ozonation process (curve c) in comparison with ozonation alone (curve a). A possible reason for this is the adsorption of ozone molecules on the catalyst surface, which resulted in further ozone decomposition and hydroxyl radical generation. Comparison of curve c and curve e of Figure 12 show that the concentration of dissolved ozone in the presence of plasma-treated catalyst is lower than that using untreated catalyst. A possible reason for this trend is the high specific surface area of CNs, which cause more ozone molecules to be decomposed on the surface.

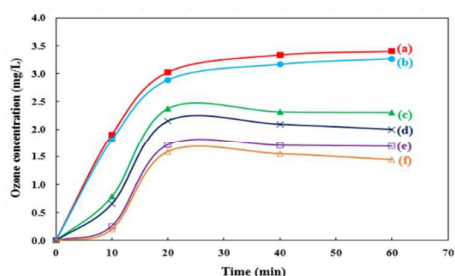


**Figure 12.** Ozone concentration in the different processes, (a) ozonation in the absence of nalidixic acid, (b) ozonation in the presence of nalidixic acid, (c) ozonation with NCMs in the absence of nalidixic acid, (d) ozonation with NCMs in the presence of nalidixic acid, (e) ozonation with CNs in the absence of nalidixic acid, and (f) ozonation with CNs in the presence of nalidixic acid (Experimental conditions:  $[\text{nalidixic acid}]_0 = 20 \text{ mg/L}$ , ozone inlet flow rate = 7 L/h,  $[\text{NCMs}] = 2 \text{ g/L}$ ,  $[\text{CNs}] = 2 \text{ g/L}$ , and  $\text{pH} = 7$ ).

### 3.3.2 The effects of various ROS scavengers

Different inorganic molecules and scavengers were applied to examine the mechanism and investigate the role of surface reactions and the main ROSs on nalidixic acid removal in the catalytic ozonation process.<sup>30</sup> The removal of nalidixic acid by the catalytic ozonation was performed in the presence of various inorganic ions and ROSs inhibitors such as *tert*-butanol (*t*-butanol),  $\text{Na}_2\text{SO}_4$ , and chloroform.<sup>40</sup> Molar ratios of scavengers to nalidixic acid of 1:1, 10:1, and 50:1 were assessed. The pseudo-first-order rate constants in the absence and presence of radical scavengers with the corresponding regression coefficients are given in Table 1.

**Table 1.** Effects of some radical scavengers on the removal efficiency of nalidixic acid by heterogeneous catalytic ozonation, (reaction conditions:  $[\text{nalidixic acid}]_0 = 20 \text{ mg/L}$ , ozone inlet flow rate = 7 L/h,  $[\text{plasma-treated clinoptilolite}] = 2 \text{ g/L}$  and  $\text{pH} = 7$ ).

Radical scavengers and their ratio	$k_{\text{app}}$ (1/min)	$R^2$
No scavenger	0.0876	0.912
[ <i>t</i> -butanol]:[nalidixic acid] = 1:1	0.0106	0.943
[ <i>t</i> -butanol]:[nalidixic acid] = 10:1	0.0069	0.940
[ <i>t</i> -butanol]:[nalidixic acid] = 50:1	0.005	0.959
$[\text{SO}_4^{2-}]$ :[nalidixic acid] = 1:1	0.0209	0.966
$[\text{SO}_4^{2-}]$ :[nalidixic acid] = 10:1	0.0115	0.957
$[\text{SO}_4^{2-}]$ :[nalidixic acid] = 50:1	0.0114	0.957
[Chloroform]:[nalidixic acid] = 1:1	0.0181	0.930
[Chloroform]:[nalidixic acid] = 10:1	0.0161	0.918
[Chloroform]:[nalidixic acid] = 50:1	0.0105	0.975

As shown in the Table 1,  $\text{Na}_2\text{SO}_4$  notably inhibits the nalidixic acid degradation in aqueous solution. When the molar ratio of

$\text{Na}_2\text{SO}_4$  to nalidixic acid is 1:1, the pseudo-first-order rate constant is 0.0209 1/min. As the molar ratio increased to 10:1 and 50:1, the rate constant gradually decreased.  $\text{SO}_4^{2-}$  ions are important hydroxyl radical scavengers, and compete with nalidixic acid molecules to react with reactive hydroxyl radicals, so the removal efficiency of the pollutant in solution is reduced in the presence of  $\text{SO}_4^{2-}$  ions.

To explain the role of hydroxyl radicals in the removal of nalidixic acid, the catalytic ozonation runs were performed in the presence of *t*-butanol as a hydroxyl radical scavenger<sup>40</sup>. In the presence of *t*-butanol at different molar ratios (1:1, 10:1, and 50:1), the removal efficiency of nalidixic acid was gradually reduced. The observed trend can be attributed to the reaction among *t*-butanol and hydroxyl radicals, which inhibits the reaction between hydroxyl radicals and nalidixic acid.

As a radical scavenger, chloroform impedes the improvement of nalidixic acid degradation. The inhibitory effect of chloroform is due to the consumption of superoxide radicals ( $\text{O}_2^{\cdot-}$ ), which can be concluded to act as an oxidizing agent in the catalytic ozonation process. The value of  $k_{\text{app}}$  is reduced to 0.0181 1/min when the molar ratio of chloroform to nalidixic acid is 1:1 and was progressively decreased as the ratio increased to 10:1 (0.0161 1/min) and 50:1 (0.0105 1/min). Accordingly, it can be proposed that the degradation of NAD is completed via the following proposed mechanism:

1. The adsorption of NAD and  $\text{O}_3$  molecule on to the surface of CNs.
2. Reaction of adsorbed ozone molecules with hydroxide ions of the catalyst surface that finally resulted in  $\text{HO}_2^{\cdot}$  molecules formation (decomposition of the ozone).
3. Generation of other reactive oxygen species by involving  $\text{HO}_2^{\cdot}$  in further reactions, which ultimately resulted in hydroxyl radicals formation.
4. Reaction of the produced hydroxyl radical with NAD and the generated intermediates on the surface of the CNs.

### 3.4. Ecotoxicological studies

Ecotoxicological study is one of the standard methods for examining the influences of contaminants in aquatic environments using aquatic plants. Cytogenetic, cytotoxic, and mutagenic effects of several chemical pollutants have been investigated by this method.<sup>30</sup> Simple structure, high growth rate, and sensitivity toward a vast number of pollutants are the advantages of using aquatic plants in this method.<sup>41, 42</sup> Figure 13 indicates the visual changes in the frond color and colony integrity of *L. minor* exposed to nalidixic acid solution subjected to different time spans of the catalytic ozonation process. The 20 mg/L initial concentration of nalidixic acid solution had the maximum toxicity. In the nalidixic acid solutions treated by the catalytic ozonation process, the toxicity reduced gradually over time, implying high efficiency of the catalytic ozonation process using CNs to reduce the toxicity of the initial nalidixic acid solution.

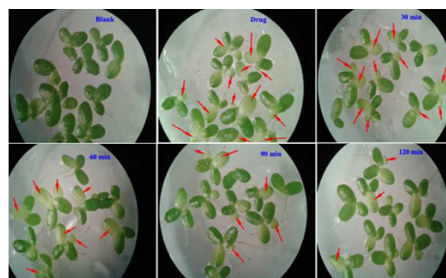


**Figure 13.** Visual changes in the fronds color of *L. minor* after 120 h (Experimental conditions:  $[\text{nalidixic acid}]_0 = 20 \text{ mg/L}$ , ozone inlet flow rate = 7 L/h,  $[\text{CNs}] = 2 \text{ g/L}$ , and  $\text{pH} = 7$ ).

### 3.5. Degradation intermediates of nalidixic acid during catalytic ozonation

The nalidixic acid degradation intermediates in the catalytic ozonation process were determined. Common peaks in GC-MS analysis were chosen and the results were evaluated by commercial standards. The results suggest that the possible nalidixic acid degradation pathway started from hydroxyl radical attack on the pyridine ring and aliphatic groups, which resulted in an aliphatic chain. Further reactions among the hydroxyl radicals and aliphatic chain resulted in the formation of amide and amine groups, which decomposed immediately, and acetic acid was formed. The proposed pathway for nalidixic acid degradation is shown in Figure 14.

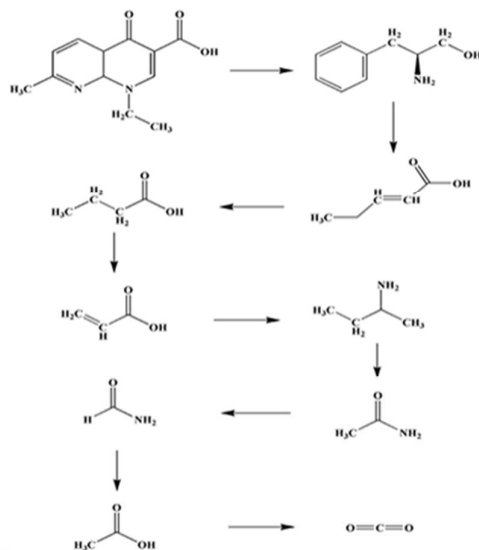


**Figure 14.** Proposed nalidixic acid degradation pathway during catalytic ozonation with plasma-treated catalyst (Experimental conditions:  $[\text{nalidixic acid}]_0 = 40 \text{ mg/L}$ ,  $[\text{CNs}] = 2 \text{ g/L}$ , ozone inlet flow rate = 7 L/h and pH = 7).

### Conclusions

CNs were produced using a GDP technique as a green technology. Physical and chemical characteristics of the catalyst were investigated using SEM, EDX, XRD, FT-IR, XPS, and BET analysis. SEM analysis results elucidated that NCMs were converted to CNs in the plasma-treatment procedure. BET analysis revealed that the specific surface area of plasma-treated catalyst increased significantly (up to 23.6 fold) after plasma-treatment. The efficiency of CNs was studied in the heterogeneous catalytic ozonation process for the removal of nalidixic acid. Under the optimum conditions of an ozone inlet flow rate of 7 L/h, catalyst concentration of 2 g/L, pH of 7, and nalidixic acid concentration of 20 mg/L, the removal efficiency was found to be 91.09%.

The mechanism of catalytic ozonation was investigated by determining the concentration of dissolved ozone and various ROS radical scavengers. The results showed that the dissolved ozone concentration in the heterogeneous catalytic ozonation process is the minimum due to the effective decomposition of ozone molecules on the active surface sites of CNs. Adding ROS radical scavengers showed the effective role of  $\cdot\text{OH}$  and  $\text{O}_2^{\cdot-}$  as the main reactive oxygen species in the removal of nalidixic acid. The investigation of the toxicity effects using an aquatic species showed that heterogeneous catalytic ozonation could notably reduce the toxicity of nalidixic acid within 120 min. Formation of intermediate

compounds with low molecular weight during 4 min of the catalytic ozonation process demonstrated the better capability of the catalytic ozonation process using CNs in the mineralization of nalidixic acid.

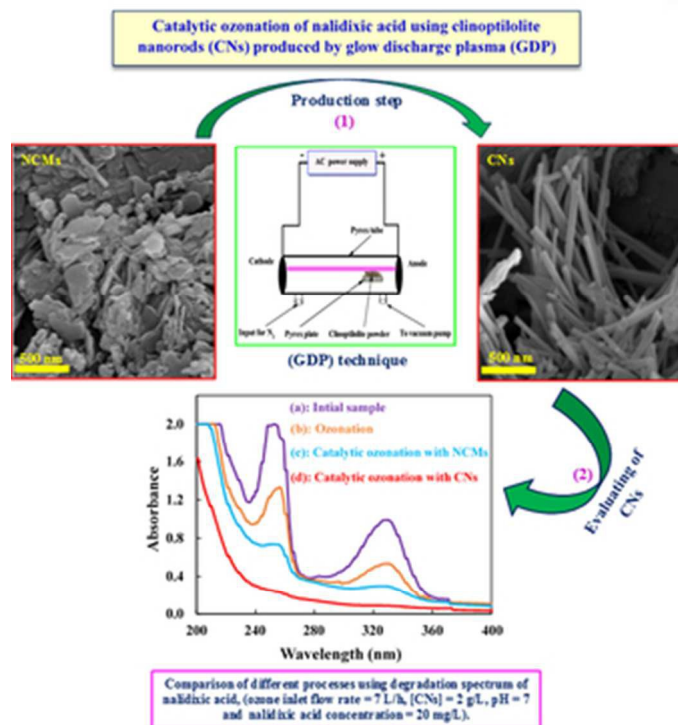
### Acknowledgements

The authors thank the University of Tabriz (Iran) for all of the guidance and support. This work is funded by the research grant NRF-2015-002423 of the National Research Foundation of Korea.

### Notes and references

- M. Fathinia, A. Khataee, A. Naseri and S. Aber, *Spectrochim. Acta, Part A*, 2015, **136**, Part C, 1275-1290.
- J. Rivera-Utrilla, M. Sánchez-Polo, M. Bautista-Toledo and J. Méndez-Díaz, *Chem. Eng. J.*, 2012, **180**, 204-209.
- A. Pal, K. Y.-H. Gin, A. Y.-C. Lin and M. Reinhard, *Sci. Total Environ.*, 2010, **408**, 6062-6069.
- A. L. Boreen, W. A. Arnold and K. McNeill, *Environ. Sci. Technol.*, 2004, **38**, 3933-3940.
- A. R. Khataee, M. Fathinia and S. W. Joo, *Spectrochim. Acta A*, 2013, **112**, 33-45.
- V. K. Gupta, I. Ali, T. A. Saleh, A. Nayak and S. Agarwal, *RSC Adv.*, 2012, **2**, 6380-6388.
- C. Sirtori, A. Zapata, W. Gemjak, S. Malato, A. Lopez and A. Agüera, *Water Res.*, 2011, **45**, 1736-1744.
- H. Yan, P. Lu, Z. Pan, X. Wang, Q. Zhang and L. Li, *J. Mol. Catal. A: Chem.*, 2013, **377**, 57-64.
- L. Yuan, J. Shen, Z. Chen and Y. Liu, *Appl. Catal., B*, 2012, **117**, 414-419.
- M. Akgul and A. Karabakan, *Micropor. Mesopor. Mat.*, 2010, **131**, 238-244.
- F. Qi, B. Xu and W. Chu, *J. Mol. Catal. A: Chem.*, 2015, **396**, 164-173.
- M. Taseidifar, A. Khataee, B. Vahid, S. Khorram and S. W. Joo, *J. Mol. Catal. A: Chem.*, 2015, **404**, 218-226.
- F. J. Beltran, F. J. Rivas and R. Montero-de-Espinosa, *Appl. Catal., B*, 2002, **39**, 221-231.
- X. Lü, Q. Zhang, W. Yang, X. Li, L. Zeng and L. Li, *RSC Adv.*, 2015, **5**, 10537-10545.
- O. Oputu, M. Chowdhury, K. Nyamayaro, F. Cummings, V. Fester and O. Fatoki, *RSC Adv.*, 2015, **5**, 59513-59521.
- F. Erol and T. A. Özbelge, *Chem. Eng. J.*, 2008, **139**, 272-283.
- C.-H. Wu, C.-Y. Kuo and C.-L. Chang, *J. Hazard. Mater.*, 2008, **154**, 748-755.
- J. Nawrocki, *Appl. Catal., B*, 2013, **142**, 465-471.
- A. Araya and A. Dyer, *J. Inorg. Nucl. Chem.*, 1981, **43**, 589-594.
- B. Legube and N. K. V. Leitner, *Catal. Today*, 1999, **53**, 61-72.
- A. Khataee, S. Bozorg, S. Khorram, M. Fathinia, Y. Hanifehpour and S. W. Joo, *Ind. Eng. Chem. Res.*, 2013, **52**, 18225-18233.
- B. Kasprzyk-Hordern, M. Ziółek and J. Nawrocki, *Appl. Catal., B*, 2003, **46**, 639-669.
- A. Ikhlaiq, D. R. Brown and B. Kasprzyk-Hordern, *Appl. Catal., B*, 2014, **154-155**, 110-122.
- L. Zeng, *Water Res.*, 2003, **37**, 4351-4358.
- C.-j. Liu, J. Zou, K. Yu, D. Cheng, Y. Han, J. Zhan, C. Ratanatawanate and B. W.-L. Jang, *Pure Appl. Chem.*, 2006, **78**, 1227-1238.
- A. Khataee, M. Taseidifar, S. Khorram, M. Sheydaei and S. W. Joo, *J. Taiwan Inst. Chem. Eng.*, 2015.
- P. Attri, B. Arora and E. H. Choi, *RSC Adv.*, 2013, **3**, 12540-12567.
- H. Bader and J. Hoigné, *Water Res.*, 1981, **15**, 449-456.
- M. Dükkancı, M. Vinatoru and T. J. Mason, *Ultrason. Sonochem.*, 2014, **21**, 846-853.
- M. Fathinia and A. Khataee, *Appl. Catal., A*, 2015, **491**, 136-154.
- M. K. Doula, *Chemosphere*, 2007, **67**, 731-740.
- I. Rodriguez-Iznaga, A. Gomez, G. Rodriguez-Fuentes, A. Benitez-Aguilar and J. Serrano Ballan, *Micropor. Mesopor. Mat.*, 2002, **53**, 71-80.

33. D. Ruiz-Serrano, M. Flores-Acosta, E. Conde-Barajas, D. Ramírez-Rosales, J. Yáñez-Limón and R. Ramírez-Bon, *J. Mol. Struct.*, 2010, **980**, 149-155.
34. R. Huang, B. Lan, Z. Chen, H. Yan, Q. Zhang and L. Li, *Chem. Eng. J.*, 2012, **180**, 19-24.
35. S. G. Ardo, S. Nélieu, G. Ona-Nguema, G. Delarue, J. Brest, E. Pironin and G. Morin, *Environ. Sci. Technol.*, 2015, **49**, 4506-4514.
36. F. Petronella, S. Diomedea, E. Fanizza, G. Mascolo, T. Sibillano, A. Agostiano, M. Curri and R. Comparelli, *Chemosphere*, 2013, **91**, 941-947.
37. A. Aguinaco, F. J. Beltrán, J. F. García-Araya and A. Oropesa, *Chem. Eng. J.*, 2012, **189-190**, 275-282.
38. F. Qi, B. Xu, L. Zhao, Z. Chen, L. Zhang, D. Sun and J. Ma, *Appl. Catal., B*, 2012, **121**, 171-181.
39. M. Sui, S. Xing, L. Sheng, S. Huang and H. Guo, *J. Hazard. Mater.*, 2012, **227**, 227-236.
40. E. M. Rodríguez, G. Márquez, M. Tena, P. M. Álvarez and F. J. Beltrán, *Appl. Catal., B*, 2014.
41. L. Li, M. Sillanpää, M. Tuominen, K. Lounatmaa and E. Schultz, *Ecotox. Environ. Safe.*, 2013, **88**, 89-94.
42. Š. Zezulka, M. Kummerová, P. Babula and L. Váňová, *Aquat. Toxicol.*, 2013, **140**, 37-47.



28x31mm (300 x 300 DPI)